Design of an Asymmetric Rotor Pole for Wound Field Synchronous Machines

Wenping Chai, *Member, IEEE,* and Byung-il Kwon, *Senior Member, IEEE*

***Abstract*—This study proposes a novel asymmetric rotor pole design for wound field synchronous machines (WFSMs), which can achieve high saliency ratio and also low torque ripple. The key point is the optimal design of the asymmetric rotor pole with the inverse-cosine-shaped (ICS) plus reverse 3rd harmonic shaping. The asymmetric rotor pole can help to improve the average output torque by enhancing the saliency ratio. The reverse 3rd harmonic shaping on the rotor pole surface is mainly used to reduce the torque ripple. To certify the effectivity of the proposed design, three-phase 54-slot / 6-pole 4.7kW WFSMs with uniform air gap and with non-uniform air gap shaped by the ICS plus optimum reverse 3rd harmonic are utilized as the basic model and referenced model for comparison. For the referenced model, the optimum amplitude of reverse 3rd harmonic is preferred as 1/6. Finally, all electromagnetic characteristics of the investigated machines are predicted by the finite-element method (FEM). The highest saliency ratio and comparatively low torque ripple have been verified.**

***Index Terms*—Asymmetric rotor pole, high saliency ratio, low torque ripple, wound field synchronous machine.**

I. Introduction

WFSMs are drawing more and more attentions due to flexible flux regulation and no magnet limited in a lot of industrial applications, such as EVs[1], steam turbines[2], wind turbines[3], et al. However, the rotor excitation by the current in rotor field coils is the main factor that produces the output torque. The current in the rotor field coils make the additional copper loss, which reduces the efficiency of WFSMs.

Some research has been studied to reduce the rotor copper loss by enhancing saliency ratio, which is beneficial to reluctance torque production [4]. One method to improve the reluctance torque is inserting flux barriers in the rotor pole, which make the rotor some segments [5]. The segmented rotor should be fixed together by special handling. Another method is using the reverse 3rd harmonic shaping function to shape the rotor pole head [6]. Due to the enlarging average air gap length caused by the reversed 3rd harmonic shaping function, the field torque will be reduced. So, the increased reluctance torque and the reduced field torque should be balanced for an optimum percentage. Without doubt, both methods are trying to decrease the *q*-axis magnetic inductance for higher saliency ratio.

Recently, the stator of the flux reversal permanent magnet (PM) machine applies the asymmetric pole configuration for improving the torque capability [7]. The consequent-pole PM machine with asymmetric magnetic pole structure is proposed to obtain the smaller torque ripple and unipolar leakage flux without worsening the torque characteristics [8]. An asymmetric modular consequent-pole rotor is adopted to a spoke-type PM machine for enhancing the effective PM flux [9]. The magnetic-field-shifting techniques are to apply the asymmetric rotor pole to interior PM machines for enhancing the torque [10][11].

However, few researches study the asymmetrical rotor for WFSMs. The two asymmetrical rotor geometries are designed for reluctance machines [12][13]. But until now, they are not applied by industry. In [14], a WFSM adopted the asymmetrical rotor geometry, but the purpose is only to simplify the assembly process and wound the rotor winding easily.

In this paper, the asymmetric rotor pole with the ICS plus reverse 3rd harmonic shaping design of a WFSM is used to achieve high saliency ratio and also low torque ripple. The detailed parameters of the rotor pole head are obtained by the optimization techniques with the combination of Kriging method and micro genetic algorithm (GA). To verify the proposed asymmetric rotor, the basic model and the referenced model with its optimum value under the same working condition and the same stator are adopted for comparison by 2-D FEM.

II. Topology and Analysis of the Machines

A. General Characteristic of the Basic WFSM

A three-phase 54 slot/6-pole 4.7kW WFSM is first selected as the basic model, which is shown in Fig.1. To highlight the influence of the rotor pole surface, the air gap between the stator inner surface and the rotor pole outer surface is uniform. And it is worth noting that the rotor pole is symmetric. Table I lists the main specifications of the basic model.

By convention, the direction of the magnetic flux that produced by the rotor excitation and the one positioned 90 electrical degrees counterclockwise from the rotor excitation magnetic flux direction are respectively defined as the *d*-axis and the *q*-axis, which has displayed in Fig.1.

Manuscript received April 09, 2021; revised May 16, 2021, July 05, 2021 and August 22, 2021; accepted October 28, 2021. date of publication December 25, 2021; date of current version December 18, 2021.

Wenping Chai is with School of New Energy, Harbin Institute of Technology at Weihai, Weihai 264209, China (e-mail: wpchai@163.com).

Byung-il Kwon is with Department of Electronic Engineering, Hanyang University, Ansan15588, South Korea(e-mail: bikwon@hanyang.ac.kr).

(Corresponding Author: Wenping Chai)

Digital Object Identifier 10.30941/CESTEMS.2021.00037

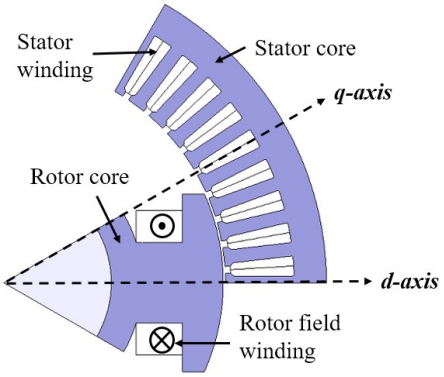

Fig. 1. Topology of the basic model.

TABLE I
MAIN DESIGN SPECIFICATIONS OF BASIC MODEL

Item	Unit	Basic
Slots/poles	-	54/6
Stator outer diameter	mm	240
Stator inner diameter	mm	165
The minimum air gap length	mm	0.85
Motor axial length	mm	123
Shaft diameter	mm	80
Magnetic motive force	A*turns	5*30
Slot filling ratio	-	0.71
Rated current	A	18
Rated speed	rpm	3000

To simply the mathematic expression, the space harmonics and winding resistances are assumed to be neglected. Therefore, under the *d*-*q* rotating reference frame, the steady-state stator voltage equations of WFSMs are expressed as:

$$\begin{cases} U_d = -\omega L_q I_q \\ U_q = \omega L_d I_d + \omega \lambda_f \end{cases} \tag{1}$$

where, U_d and U_q are the terminal voltages in the *d*-axis and the *q*-axis, respectively; ω is the electrical speed; I_d and I_q are the armature currents; L_d and L_q are the inductances; λ_f is the field magnetic flux linked with the armature winding in the *d*-axis.

The armature currents under the *d*-*q* rotating reference frame are listed as:

$$\begin{cases} I_d = -I_S \sin\delta \\ I_q = I_S \cos\delta \end{cases} \tag{2}$$

where, δ is the current phase angle, and I_s is the peak value of the phase current.

The corresponding electromagnetic torque can be obtained as follows:

$$T_e = \frac{3p}{2}\left[\lambda_f I_q + \left(L_d - L_q\right) I_d I_q\right] \tag{3}$$

where, p is the number of pole pairs. The first term in (3) is from the rotor excitation and called as the field torque, and the second one is from the saliency between the *d*- and *q*- axis inductances and called as the reluctance torque. Due to the structure of WFSMs, L_d is bigger than L_q and the saliency ratio of WFSMs is defined as L_d/L_q. Therefore, when the current phase angle of WFSMs is controlled with $-90° < \delta < 0°$, the field torque and the reluctance torque are reinforcing. In this case, the reluctance torque can be increased with the enhancement of the saliency ratio, which benefits for the output torque.

B. Referenced Model with ICS+reverse 3rd Harmonic Shaping

Reference [6] proposed a rotor pole head surface design with the ICS plus reverse 3rd harmonic to form non-uniform air gap. And then, the sinusoidal air-gap flux density distribution with 3rd harmonic component are obtained for low torque ripple. The variation of air gap length l_{gx} with shaped-arc angle x is shown in Fig.2, which is limited by the equation (4).

$$l_{gx}(x) = \frac{\kappa * l_g}{\cos(\pi x/\tau) + a * \cos(3 * \pi x/\tau)} \tag{4}$$

where, l_g is the minimum air gap length, τ is the pole pitch. The position with x=0 is assumed at the center of the magnetic pole. The minimum air gap length is kept as a constant by the coefficient k. a decides the amplitude of the reverse 3rd harmonic. According to the equation (4), when the x is closed to $\tau/2$, the average air gap length is longest, and when the x is 0, the rotor pole is same to that of the basic model.

Furthermore, the minimum air gap length is fixed as the average air gap length of the basic model, meanwhile the shaping function will help to determine the other position of the air gap length. Finally, the optimum a is preferred as 1/6, which is selected as the referenced model in this study for comparison. The topology of the referenced model is displayed as Fig.3. For fair comparison, all parts of the referenced model are kept same with that of the basic model except the rotor pole head surface.

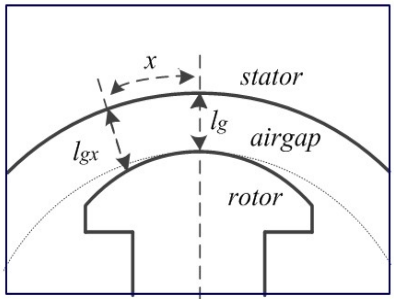

Fig. 2. The rotor pole head surface of the referenced model.

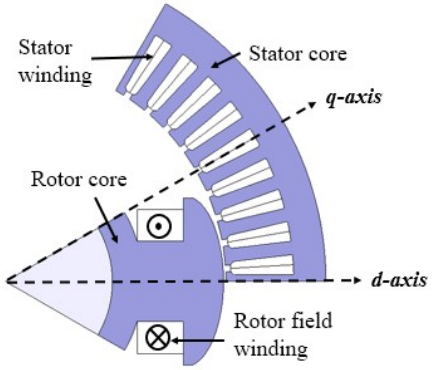

Fig. 3. Topology of the referenced model.

C. Proposal of the Asymmetric Rotor

The magnetic flux distribution of the referenced model under

different load conditions have been checked by FEM as shown in Fig.4. It can be found that the right part of the rotor pole head has very low magnetic flux with the rated load, which means the right part of the rotor pole head has low effect on the field torque.

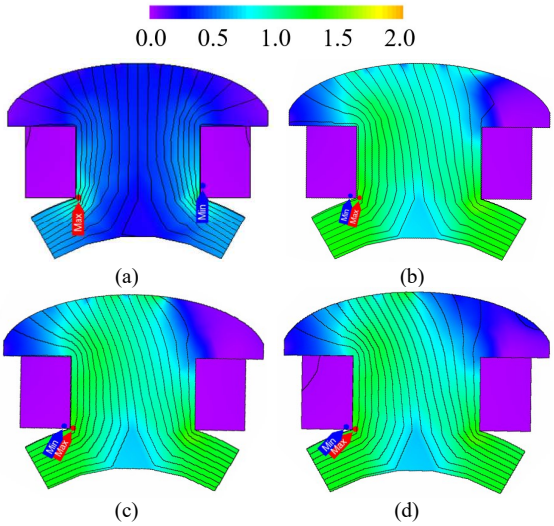

Fig. 4. Magnetic flux distribution of the referenced model under different conditions (a) no load (b) rated load with 0˚phase current (c) rated load with 45˚ phase current (d) rated load with 90˚phase current.

However, because the relative magnetic permeability of the iron and air have much difference, removing the right part of the rotor pole head, which is in the *q*-axis flux loop, will directly affect the magnetic inductance of the *q*-axis and therefore the reluctance torque. Next, the related effect is analyzed in theory [15]. But clearly, when removing the right part of the rotor pole head, the proposed asymmetric rotor pole is formed, which is designed to operate unidirectional.

Fig.5 shows the equivalent magnetic circuits of the WFSM in *d*-*q* axis, which neglect the magnetic reluctance of iron core and the stator slots. F_{dg} and F_{qg} are the stator magnetomotive force of the *d*-axis and the *q*-axis as expressed in equation (5).

$$\begin{cases} F_{dg} = NI_d \\ F_{qg} = NI_q \end{cases} \tag{5}$$

where, *N* is the turns number of winding.

The air gap magnetic reluctances in the *d*-axis and the *q*-axis can be expressed as following.

$$R_{dg1}+R_{dg2} = \frac{l_d}{\mu_0\mu_r A_{dg}} \tag{6}$$

$$R_{qg1}+R_{qg2} = \frac{l_q}{\mu_0\mu_r A_{qg}} \tag{7}$$

where u_0 is the magnetic permeability of vacuum, l_d and l_q are the air gap length in *d*-axis flux loop and *q*-axis flux loop, and A_{dg} and A_{dg} is the cross-sectional area of the air gap in the *d*-axis and *q*-axis, u_r is the relative magnetic permeability of air.

The inductances of the *d*-axis and *q*-axis can be expressed as following.

$$L_d = \frac{N\phi_d}{I_d} = \frac{N^2}{R_{dg1}+R_{dg2}} = \frac{N^2\mu_0\mu_r A_{dg}}{l_d} \tag{8}$$

$$L_q = \frac{N\phi_q}{I_q} = \frac{N^2}{R_{qg1}+R_{qg2}} = \frac{N^2\mu_0\mu_r A_{qg}}{l_q} \tag{9}$$

So, the saliency ratio is shown as:

$$\frac{L_d}{L_q} = \frac{A_{dg}l_q}{A_{qg}l_d} \tag{10}$$

The proposed asymmetric rotor is formed by shortening the right part of the rotor pole head as shown in Fig.6. The A_{gq} and l_d are less affected by the proposed asymmetric rotor, so they can be assumed as constants. In Fig.7, the radian of the full rotor pole head and the shortened part is α (*rad.*) and β (*rad.*), respectively. The radius of the rotor is *r*, and the motor axial length is l_a. Hence, A_{gd} is expressed as:

$$A_{dg} = l_a r\alpha \tag{11}$$

For the proposed asymmetric rotor, A_{gd} and l_q can be re-written as:

$$A'_{dg} = l_a r(\alpha-\beta) \tag{12}$$

$$l'_q = l_q + \beta r \tag{13}$$

Therefore,

$$A_{dg}l_q - A'_{dg}l'_q = l_a r\alpha l_q - l_a r(\alpha-\beta)(l_q+\beta r) = l_a\beta r\left[l_q-(\alpha-\beta)r\right] \tag{14}$$

It is clear to see $A_{dg}l_q < A'_{dg}l'_q$, so the saliency ratio can be increased by the asymmetric rotor.

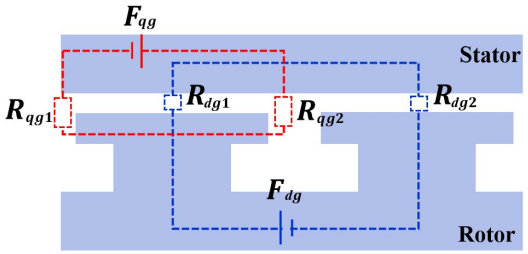

Fig. 5. Equivalent magnetic circuits of the basic WFSM in *d*-*q* axis

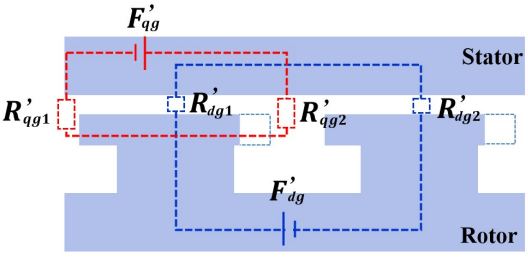

Fig. 6. Equivalent magnetic circuits of the WFSM with an asymmetric rotor in *d*-*q* axis

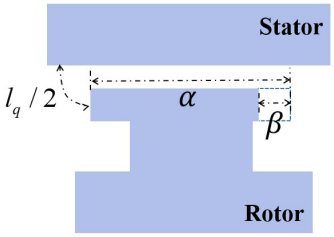

Fig. 7. The part of WFSM with an asymmetric rotor

D. Summary

Based on the above-mentioned investigation, it can be

concluded that the rotor pole head surface with the ICS plus reverse 3rd harmonic benefits with the torque ripple reduction, and the positive influence of the asymmetric rotor on the saliency ratio and reluctance torque of the WFSM. However, both the rotor pole heads surface shaping method and the asymmetric rotor reduce the average length of the air gap, which will decrease the field torque. Due to the magnetic saturation and the complicated structure, it is not easy to determine the design parameters by the theoretical method. Therefore, the optimal technique combined with the Kriging method and the micro GA is utilized to obtain the better output performance.

III. Proposed Model and Optimal Design

A. The Proposed Model with the Asymmetric Rotor and ICS + Reverse 3rd Harmonic Shaping

Hence, the asymmetric rotor is adopted in the proposed model. And to keep low torque ripple, the surface of the asymmetric rotor pole head is still shaped by equation (4). For better air gap flux density distribution, the position of the minimum air gap length is always the center of the rotor pole head arc, which is affected by the shortened part. So, the proposed model is presented in Fig.8. It should be noted that the asymmetric rotor can improve the reluctance torque, but the rotor pole surface with ICS + reverse 3rd harmonic shaping will cause the increase of l_d, which is bad for the field torque. Therefore, to balance the design parameters and obtain better performance with high saliency ratio and low torque ripple, the main variables related to the proposed asymmetric pole head shape should be designed by an optimization procedure. It should be mentioned that all the design parameters are kept the same with the basic model and referenced model besides the rotor pole head surface for fair comparison.

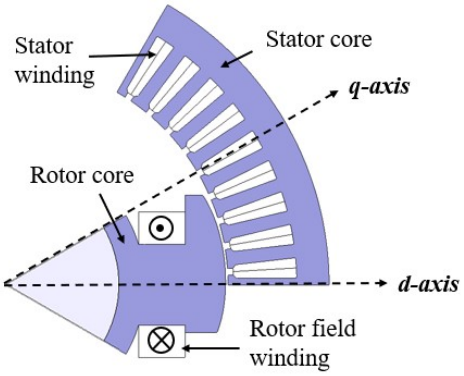

Fig. 8. Topology of the proposed model the asymmetric rotor and reverse 3rd harmonic shaping.

B. Optimization Procedure

Fig.9 summarizes the optimization procedure [16] [17], which will be carried out for the proposed model. First, based on the requirements of the proposed model, determine the objective functions, the design variables and the constraints; Second, design a series of experiments for selecting the sampling points by the Latin hypercube sampling method, simulate each sample model by FEM and obtain their performances; Then, build the approximation modeling by the Kriging method; Next, utilize the micro GA to evaluate the fitness according to the function developed by the Kriging method, and the optimal results including the values of the design variables and the predicted objective values can be obtained by the population. Finally, the values of the design variables in the optimal results are used in the simulation by the FEM. If the results are similar to the predicted value and satisfy the target, the process is completed; If not, the design variables will be adjusted, and the optimization procedure should be carried out again.

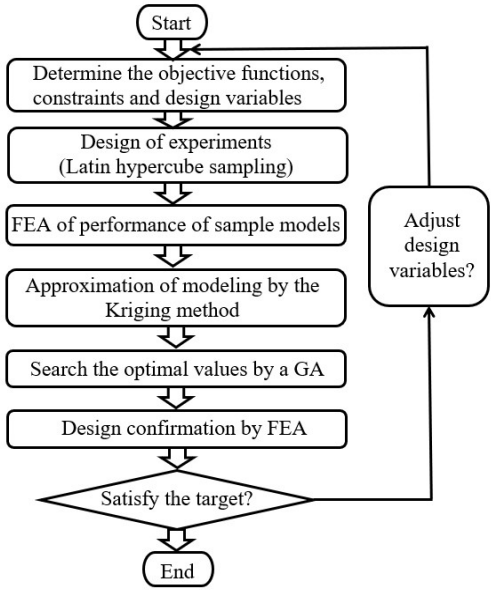

Fig. 9. Optimal design process [16].

Equation (15) lists the objective functions, which are maximizing the average torque and minimizing the torque ripple. Equation (16) lists the constraints. Fig.10 shows the design variables of the proposed asymmetric rotor. One is a, which is the amplitude of the reverse 3rd harmonic that is used to inject into the ICS rotor. The other one is t, which affects the asymmetric pole head. Equation (17) lists the ranges of the design variables.

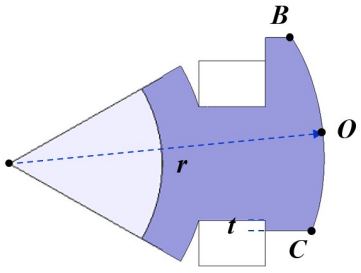

** O is the center of $\widehat{BC}$.*

Fig. 10. Design variables of the proposed asymmetric rotor.

Objective Function: (15)

Maximizing average torque
Minimizing torque ripple

Constraints: (16)

r = 81.65mm

$$\widehat{BO} = \widehat{CO}$$

Design variables: (17)

$$0 \le t \le 18.21\text{mm}$$
$$0 \le a \le 0.4$$

In the optimization procedure, the same weighting value is assigned to the two objective functions. Table II lists the convergence results of the design variables and objective values that obtained from the GA, which have been confirmed by the FEM.

TABLE II
OPTIMAL RESULTS OF THE PROPOSED MODEL

Item		Unit	Value
t		mm	2.743
a		mm	0.125
Predicted objective value by GA	Torque	Nm	16.960
	Torque ripple	%	7.326
Calculated objective value by FEM	Torque	Nm	16.961
	Torque ripple	%	7.187

IV. PERFORMANCE COMPARISON

To demonstrate the validity of the proposed asymmetric rotor with the ICS + reverse 3rd harmonic shaping, the FEM was utilized to investigate the electromagnetic performance of the optimal model in detail. For fair comparison, the electromagnetic performance of the basic model and referenced model, which share the same stator, were also investigated.

A. No-load Performances

Under the no-load condition, the air gap flux densities of the basic model, referenced model and the optimal model are investigated as shown in Fig.11. It can be seen that the referenced model and the optimal model can achieve waveform of the air gap flux densities more sinusoidal. For a clear view, the corresponding back EMF waveforms in one phase of each model are all drawn in Fig. 12 (a). Fig.12 (b) shows the FFT results of each back EMF waveform. It can be seen that both the referenced model and the optimal model can effectively reduce the 9th, 11th, 13rd, 15th and 17th harmonic, compared to that of basic model. The fundamental harmonics of the referenced model and optimal model are similar, which verifies that the asymmetric rotor proposed in section II.C has less effect on the field torque, but both are less than that of the basic model, which is due to the air gap length enlarged by the ICS + reverse 3rd harmonic shaping.

B. Torque Component Characteristics

In the simulation, the three-phase sinusoidal current as the power source excites the stator windings to obtain electromagnetic torques. Next is to separate the field torque and reluctance torque. First, the total torque is simulated; Then the rotor excitation is set as zero, and the frozen permeability method [18] was utilized to fix the permeability of the iron core as that in the first step, so the reluctance torque is obtained. Third, the field torque is obtained from the total torque minus the reluctance torque. The torque characteristics of the basic

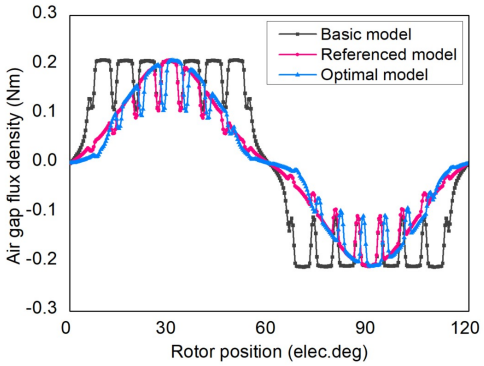

Fig. 11. Air gap flux densities.

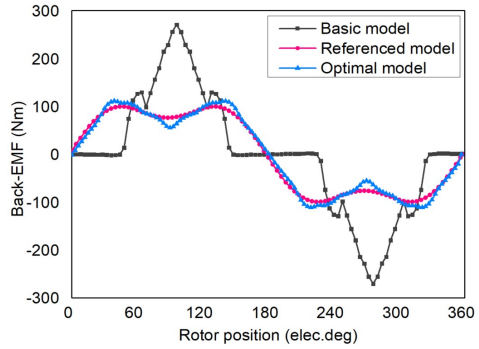

(a)

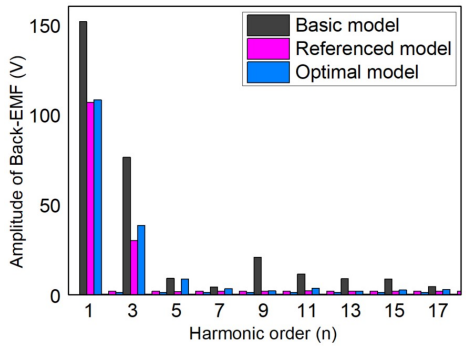

(b)

Fig. 12. Back-EMF in one phase (a) waveform (b) FFT.

model, referenced model and optimal model are predicted by FEM as shown in Fig.13. Table III gives the details of the comparisons of electromagnetic performance.

The field torques and the reluctance torques of all the models as shown in Fig.13(a)~(c), reached their maximal values at the 45 electrical degree difference current-phase angles. The saliency ratio of the optimal model was improved by 42.4% and 7.9%, respectively, compared to the basic model and the referenced model. Correspondingly, the reluctance torque is increased with the increase of the saliency ratio. As the increase of the average air gap length, the field torque of the optimal model was still decreased, compared to that of the basic model. But compared to that of the referenced model, the field torque has a little relief. Fortunately, the balance between the increase of the reluctance torque and the decrease of the field torque has been found in the optimal model. It shows that the better performance has been got, compared with the referenced model. The ratios of the reluctance torque to the average torque of three models are 22.4%, 52.8% and 55.1%, respectively. This means

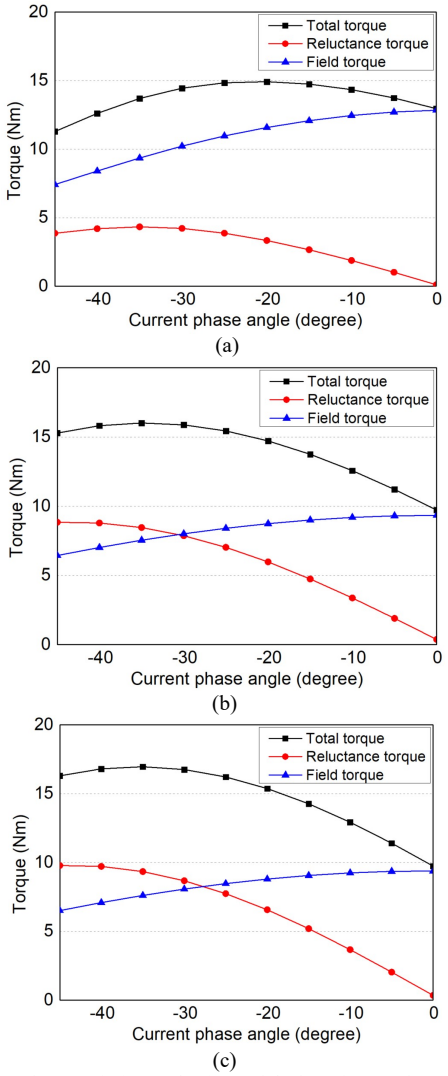

Fig.13. Torque characteristics (a) basic model. (b) referenced model. (c) optimal model.

when the rotor excitation is failure, the optimal model can still guarantee a certain percentage of the output torque, which reduce the risk of the sudden stop.

The maximum total torque varied with the rotor position of the three models are shown in Fig. 14. It can be clearly seen that the average torque of the optimal model is highest in three models. Compared with the basic model, the torque ripple of the optimal model is reduced by 92.97%. However, compared with the referenced model, the torque ripple of the optimal model is lightly increased, but 7.19% is real a low value [19] for these kinds of machines along with the enhanced saliency ratio.

The output power of the optimal model is increased with the increase of the average torque, due to the improvement of reluctance torque. Consequently, the efficiency of the optimal model is 91.8%, which is the highest compared to that of the basic model and the referenced model. The efficiency is herein estimated by

$$Efficiency = \frac{output\ \ power}{output\ \ power + losses} \tag{18}$$

The losses in this section only consider the main losses including the simulated iron loss and the calculated copper loss.

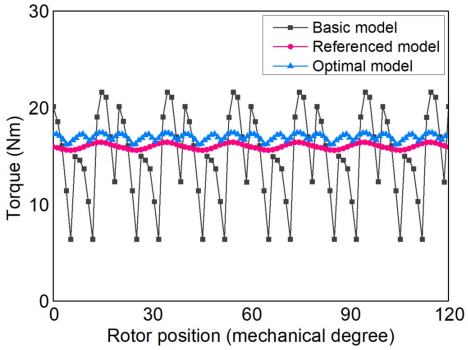

Fig.14. Comparison of maximum electromagnetic torques.

TABLE III
PERFORMANCE COMPARISON OF THE INVESTIGATED MODELS

Item	Unit	Basic	Referenced	Optimal
Back-EMF (RMS)	V	121.87	79.28	81.85
Average torque	Nm	14.92	16.01	16.96
Reluctance torque	Nm	3.34	8.46	9.35
Field torque	Nm	11.58	7.55	7.61
Saliency ratio	--	1.25	1.65	1.78
Torque ripple	%	102.3	5.10	7.19
Cogging torque	Nm	0.584	0.002	0.006
Power @3000rpm	kW	4.687	5.029	5.327
Efficiency @3000rpm	%	90.8	91.4	91.8

V. CONCLUSION

This study proposed a novel WFSM with a novel asymmetric rotor pole design. By the analysis of the optimal design based on the micro GA, the optimal model is obtained and the performance is verified by the FEM. As the results show, the saliency ratio of the optimal model is increased by 42.4% and 7.8%, respectively, compared to that of the basic model and the referenced model, the average torque is increased by 13.67% and 5.9%, which benefits of the enlarged saliency ratio. And the 3rd harmonic shaping on the asymmetric rotor pole surface help to decrease the torque ripple by 92.97% compared to that of the basic model, though a little worse than that of the referenced model.

REFERENCES

[1] H. Park, and M. Lim. "Design of High-Power Density and High Efficiency Wound-Field Synchronous Motor for Electric Vehicle Traction." *IEEE Access*, vol.7, pp.46677-46685, Mar. 2019.

[2] J. Daley., R. Siciliano. "Application of emergency and standby generation for distributed generation. I. Concepts and hypotheses", *IEEE Trans. Ind. Appl.*, vol. 39, no.4, pp. 1214–1225, 2003.

[3] N. S. Hasan, M. Y. Hassan, M. S. Majid, and H. A. Rahman, ''Review of storage schemes for wind energy systems," *Renew. Sustain. Energy Rev.*, vol. 21, pp. 237–247, May 2013.

[4] W. Chai, H. Yang, F. Xing, B. Kwon. "Analysis and Design of a PM-assisted Wound Rotor Synchronous Machine with Reluctance Torque Enhancement," *IEEE Trans. Ind. Electron.*, vol. 68, no. 4, pp. 2887-2897, April 2021.

[5] W. Chai, W. Zhao, and B.-I. Kwon, "Optimal design of the wound field synchronous reluctance machines to improve torque by increasing saliency ratio," *IEEE Trans. Magn.,* vol. 53, no. 11, Nov. 2017, Art. no. 8103205.

[6] W. Chai and B. Kwon, "Saliency Enhancement and Torque Ripple Reduction of Wound Field Synchronous Machine by Injecting Optimum

Harmonic in Rotor Shape," *Int. J. Appl. Electrom.*, vol. 64, no. 1-4, pp. 447-455, Aug. 2020.

[7] H. Yang, H. Lin, Z. Q. Zhu, S. Lyu, and Y. Liu, "Design and analysis of novel asymmetric-stator-pole flux reversal PM machine," *IEEE Trans. Ind. Electron.*, vol. 67, no. 1, pp. 101–114, Jan. 2020.

[8] F. Li, K. Wang, J. Li, and H. Y. Sun, "Electromagnetic performance analysis of consequent-pole PM machine with asymmetric magnetic pole," *IEEE Trans. Magn.*, vol. 55, no. 6, Jan. 2019, Art. no. 8103205.

[9] J. Li and K. Wang, "A Novel Spoke-Type PM Machine Employing Asymmetric Modular Consequent-Pole Rotor," *IEEE/ASME Trans. Mech.*, vol. 24, no. 5, pp. 2182-2192, Oct. 2019.

[10] Z. Q. Zhu and Y. Xiao, "Novel Magnetic-field-shifting Techniques in Asymmetric Rotor Pole Interior PM Machines with Enhanced Torque Density," *IEEE Trans. Magn.*, Early Access Article, 03 May 2021.

[11] Y. Xiao et al., "A Novel Asymmetric Interior Permanent Magnet Machine for Electric Vehicles," *IEEE Trans. Energy Convers*, 29 January 2021.

[12] G. Li, J. Ojeda, S. Hlioui, et al. "Modification in rotor pole geometry of mutually coupled switched reluctance machine for torque ripple mitigating," *IEEE Trans. Magn.*, vol. 48, no.6, pp. 2025–2034, 2012

[13] Aspden H. "Magnetic reluctance motor," UK Patent GB2303255A, 1997.

[14] N. Yang, W. Cao, Z. Liu, J. Morrow, "Design of an asymmetrical rotor for easy assembly and repair of field windings in synchronous machines," *The Journal of Engineering*, vol.8, pp.427-434, 2017.

[15] Slobodan N. Vukosavic "Electrical Machines," in Power Electronics & Power Systems, New York, USA: Springer Science + Business Media, 2013.

[16] J. B. Kim, K. Y. Hwang, and B. I. Kwon, "Optimization of two-phase in-wheel IPMSM for wide speed range by using the Kriging model based on Latin hypercube sampling," *IEEE Trans. Magn.,* vol. 47, no. 5, pp. 1078–1081, May 2011.

[17] W. Chai, T. A. Lipo, B. I. Kwon, "Design and Optimization of a Novel Wound Field Synchronous Machine for Torque Performance Enhancement," *Energies*, vol.11, no.8, pp.2111, 2018.

[18] J. A. Walker, D. G. Dorrell, and C. Cossar, "Flux-linkage calculation in permanent-magnet motors using the frozen permeabilities method," *IEEE Trans. Magn.*, vol. 41, no. 10, pp. 3946–3948, Oct. 2005.

[19] F. Guo, M. Salameh, M. Krishnamurthy and I. P. Brown, "Multimaterial Magneto-Structural Topology Optimization of Wound Field Synchronous Machine Rotors," *IEEE Trans. Ind. Appl.*, vol. 56, no. 4, pp. 3656-3667, July-Aug. 2020.

WENPING CHAI (M'16) was born in Liaoning, China, in 1991. She received the B.S. degrees in electrical engineering and automation and also management from the Harbin Institute of Technology, in 2014, and the Ph.D. degree in electrical engineering from the Department of Electrical and Electronic Engineering, Hanyang University, South Korea, in 2020. She is currently an Assistant Professor of electrical engineering with the School of New Energy, Harbin Institute of Technology at Weihai, Weihai, China. Her research interest includes the design, analysis, and optimization of electric machines.

BYUNG-IL KWON (SM) was born in 1956. He received the B.S. and M.S. degrees in electrical engineering from Hanyang University, Ansan, South Korea, in1981and1983, respectively, and the Ph.D. degree in electrical engineering, machine analysis from The University of Tokyo, Tokyo, Japan, in 1989. From 1989 to 2000, he was a Visiting Researcher with the Faculty of Science and Engineering Laboratory, University of Waseda, Tokyo. In 1990, he was a Researcher with the Toshiba System Laboratory, Yokohama, Japan. In 1991, he was a Senior Researcher with the Institute of Machinery and Materials Magnetic Train Business, Daejeon, South Korea. From 2001 to 2008, he was a Visiting Professor with the University of Wisconsin–Madison, Madison, WI, USA. He is currently a Professor with Hanyang University. His research interest includes the design and control of electric machines.